Published in final edited form as:
Cancer Res. 2011 May 15; 71(10): 3459–3470. doi:10.1158/0008-5472.CAN-10-2999.

Role for Stromal Heterogeneity in Prostate Tumorigenesis

Maria A. Kiskowski[1,*], **Roger S. Jackson 2nd**[2,3,*], **Jheelam Banerjee**[2,3], **Xiaohong Li**[2,3], **Minchul Kang**[4], **Juan M. Iturregui**[2,5], **Omar E. Franco**[2,3], **Simon W. Hayward**[2,3], and **Neil A. Bhowmick**[6,**]

[1]Department of Mathematics and Statistics, University of South Alabama, Mobile, AL

[2]Vanderbilt-Ingram Cancer Center, Vanderbilt University School of Medicine, Nashville, TN

[3]Department of Urologic Surgery, Vanderbilt University School of Medicine, Nashville, TN

[4]Department of Molecular Physiology and Biophysics, Vanderbilt University School of Medicine, Nashville, TN

[5]Department of Pathology, Vanderbilt University School of Medicine, Nashville, TN

[6]Department of Medicine, Cedars-Sinai Medical Center, Los Angeles, CA

Abstract

Prostate cancer develops through a stochastic mechanism whereby pre-cancerous lesions on occasion progress to multifocal adenocarcinoma. Analysis of human benign and cancer prostate tissues revealed heterogeneous loss of TGF-β signaling in the cancer associated stromal fibroblastic cell compartment. To test the hypothesis that prostate cancer progression is dependent on the heterogeneous TGF-β responsive microenvironment, a tissue recombination experiment was designed where the ratio of TGF-β responsive and nonresponsive stromal cells were varied. While 100% TGF-β responsive stromal cells supported benign prostate growth and 100% TGF-β non-responsive stromal cells resulted in pre-cancerous lesions, only the mixture of TGF-β responsive and nonresponsive stromal cells resulted in adenocarcinoma. A computational model was used to resolve a mechanism of tumorigenic progression where proliferation and invasion occur in two independent steps mediated by distinct stromally derived paracrine signals produced by TGF-β non-responsive and responsive stromal cells. Complex spatial relationships of stromal and epithelial cells were incorporated into the model based on experimental data. Informed by incorporation of experimentally derived spatial parameters for complex stromal-epithelial relationships, the computational model indicated ranges for the relative production of paracrine factors by each cell type and provided bounds for the diffusive range of the molecules. Since SDF-1 satisfied model predictions for an invasion promoting paracrine factor, a more focused computational model was subsequently used to investigate if SDF-1 was the invasion signal. Simulations replicating SDF-1 expression data revealed the requirement for cooperative SDF-1 expression, a prediction supported biologically by heterotypic stromal IL-1β signaling between fibroblastic cell populations. The cancer stromal field effect supports a functional role for the unaltered fibroblasts as a cooperative mediator of cancer progression.

** Address correspondence to: Neil A. Bhowmick, Ph.D., Department of Medicine, Samuel Oschin Comprehensive Cancer Institute, Cedars-Sinai Medical Center, 8750 Beverly Blvd., Atrium 103, Los Angeles, CA 90048, Tel: (310) 423-5992, Fax: (310) 423-8543, bhowmickn@cshs.org.
*Both authors contributed equally.

Keywords

Prostate Tumorigenesis; Stromal-Epithelial Interactions; TGF-β; Paracrine Signaling; Computational Modeling; Cancer field effect

INTRODUCTION

Organ development and epithelial tumor progression are the result of reciprocal and sequential stromal-epithelial interactions. Prostate cancer (PCa), the most common non-cutaneous cancer in men, is initiated by the transformation of luminal epithelial cells that line the prostatic ducts resulting in altered proliferation leading to prostatic intra-epithelial neoplasia (PIN) (2). Loss of cell polarity and invasion through the basement membrane into the surrounding prostatic stroma by the transformed epithelia mediates the establishment of prostatic adenocarcinoma. The sequential progression of epithelial differentiation to adenocarcinoma is dictated by its inherent genetic stability as well as the cues provided by the surrounding microenvironment (3–5). Tgfbr2^{fspKO} mice, with a conditional knockout (KO) of the transforming growth factor beta (TGF-β) type II receptor (TβRII) gene (*Tgfbr2*) in stromal fibroblasts, develop PIN lesions and subsequently prostate adenocarcinoma (6, 7). Human PCa is analogously associated with the heterogeneous loss of TβRII expression in the stromal compartment (7, 8).

We used a flexible, biologically intuitive, hybrid computational model to investigate mechanisms for cell-cell communication in stromal and epithelial compartments on tumor initiation and progression. Hybrid mathematical modeling has developed into a means of explaining biologic mechanisms, combining explicit cell representations with continuum-based biological descriptions (11, 14–16). Our hybrid computational model combines a discrete model for the differentiation of individual epithelial cells with a continuum model of stromally derived signaling factor diffusion. Secreted signaling factors in this study include paracrine factors (that traverse the basement membrane between the stroma and the epithelia) and heterotypic stromal signaling factors (that communicate between populations of fibroblastic cells). Herein we report that biological experiments (i*n vivo* tissue recombination and *in vitro* biological models) and computational mathematical modeling together test and support hypotheses for inter-cellular signaling within a heterogeneous prostatic stromal compartment and prostatic epithelial progression to adenocarcinoma.

QUICK GUIDE TO EQUATIONS & ASSUMPTIONS

Our computational model couples a discrete, stochastic description of cells at the macroscopic scale with a continuous, deterministic description of paracrine factor diffusion at the microscopic scale.

Discrete, Stochastic Description of Cells

A spatially explicit model for cell positions incorporates the spatial scales of epithelial and stromal cells located at discrete lattice locations based on their positions in a histologic cross-section of mouse prostate (epithelia circumscribing prostate ducts surrounded by stromal fibroblastic cells. Fibroblasts were randomly identified as dominant point sources for either M_1 or M_2 paracrine factors, with probabilities depending upon the simulated fraction of WT and Tgfbr2-KO fibroblasts, respectively.

Paracrine Factor Production

Forty-four stromal cells were point sources for paracrine factors M_1 and M_2. We denote the set of wild-type (normal (N)) and Tgfbr2-KO (altered (A)) stromal cell positions as S_N and S_A in locations $S_N = \{(x_i, y_i) \mid i = 1,2,\ldots,n\}$ and $S_A = \{(\bar{x}_i, \bar{y}_i) | i = 1,2,\ldots,a\}$ with $n + a = 44$. Let m_1 and m_2 be the concentrations (μM) of paracrine factors M_1 and M_2, respectively. M_1 and M_2 are dominantly produced by Tgfbr2-KO and WT fibroblastic cells, respectively, and their production rates ($\partial m_1/\partial t$ and $\partial m_2/\partial t$) are proportional to the number of Tgfbr2-KO cells and WT cells.

Paracrine Factor Diffusion

To model diffusion in the context of the complex geometry of the mouse prostate, paracrine factors diffuse in the region between and surrounding (but not within) irregularly shaped ducts. In normal prostate, the basement membrane provides a diffusion barrier between epithelial and stromal cells. The effect of the basement membrane as a barrier to diffusion and the erosion of the basement membrane were not modeled here. Instead, the model considers the steady-state levels of paracrine factors and their effect on epithelial cells with the assumption that any erosion of the basement membrane had already occurred. Since M_1 and M_2 diffuse freely in the inter-ductal space, with certain metabolic decay rates, the kinetics of m_1 and m_2 can be described as uncoupled reaction diffusion:

$$\frac{\partial m_1}{\partial t} = k_1 \sum_{i=1}^{n} \delta(x_i, y_i) - k_{d1} m_1 + D_1 \nabla^2 m_1$$

$$\frac{\partial m_2}{\partial t} = k_2 \sum_{i=1}^{a} \delta(\bar{x}_i, \bar{y}_i) - k_{d2} m_2 + D_2 \nabla^2 m_2$$

Equation Set 1:

Here k_1 and k_2 are production rates (μm s^{-1}), k_{d1} and k_{d2} are decay rates (μm s^{-1}), and D_1 and D_2 are the diffusion coefficients ($\mu m^2/s$) of paracrine factor M_1 and M_2, respectively. The Dirac delta function $\delta(x_i,y_i)$ is defined as: $\delta(x_i, y_i) = \begin{cases} \infty & if\,(x, y) = (x_i, y_i) \\ 0 & otherwise \end{cases}$ The initial conditions for Eq. 1 were given by $m_1(x,y,0) = 0$ and $m_2(x,y,0) = 0$. No-flux boundary conditions on the ducts and the outer rectangle are given by:

$$\frac{\partial m_1}{\partial n} = 0$$

$\frac{\partial m_2}{\partial n} = 0$, where n indicates the outward facing normal of the boundary

Paracrine Factor Response

Epithelial cells respond to paracrine factors by transforming from normal to proliferative at threshold levels of M_1 and from proliferative to invasive at threshold levels of M_2. Levels of paracrine factors are measured at steady state concentrations. This simplification is justified if the time scales of epithelial transformation are much slower than the time scales of paracrine factor diffusion, which is reasonable as diffusive factor steady state concentrations establish at fast time scales compared to cellular responses (17, 18). Normal (*N*), proliferative (*P*) and invasive (*I*) cells are labeled as E_N, E_P, and E_I and their concentrations are labeled as e_n, e_p, and e_i (μM). For the time scales of e_n, e_p, and e_i, we consider m_1 and m_2 in their quasi-steady states, m_1^∞ and m_2^∞. For m_1^∞ and m_2^∞, we solve the steady state equations (from Equation Set 1):

$$D_1\nabla^2 m_1^\infty = k_{d_1} m_1^\infty - k_1 \sum_{i=1}^{a} \delta_{(x_i,y_i)}$$
$$D_2\nabla^2 m_2^\infty = k_{d_2} m_2^\infty - k_2 \sum_{i=1}^{n} \delta_{(\bar{x}_i,\bar{y}_i)}$$

Equation Set 2:

Next, the proposed underlying mechanism for epithelial transformation can be written:

$$E_N + M_1^* \rightarrow E_P$$
$$E_P + M_2^* \rightarrow E_I$$

Equation Set 3:

for quasi-steady paracrine factor levels M_1^* and M_2^* that were above threshold levels T_{M1} and T_{M2}. Therefore, the proposed two-step mechanism for cancer progression was as follows:

$$E_N \xrightarrow{M*_1} E_P \xrightarrow{M*_2} E_I \tag{3b}$$

On the other hand, for M_1° and M_2° below threshold levels:

$$E_N + M_1^\circ \rightarrow E_N$$
$$E_P + M_2^\circ \rightarrow E_P \tag{3c}$$

Assuming E_N, E_P, and E_I were immobile around the ducts, the kinetics of e_n, e_p, and e_i can be written:

$$\frac{de_n}{dt} = -k_N \cdot H(m_1^\infty - m_1^*) \cdot m_1^\infty \cdot e_n$$
$$\frac{de_p}{dt} = -k_P \cdot H(m_2^\infty - m_2^*) \cdot m_2^\infty \cdot e_p + k_N \cdot H(m_1^\infty - m_1^*) \cdot m_1^\infty \cdot e_n$$
$$\frac{de_i}{dt} = k_P \cdot H(m_2^\infty - m_2^*) \cdot m_2^\infty \cdot e_p$$

Equation Set 4:

where k_N and k_P were transformation rate constants of M_1 and M_2 to E_N and E_P. The Heaviside function $H(x)$ was defined as: $H(x) = \begin{cases} 0 & x<0 \\ 1 & x \geq 0 \end{cases}$. Because the total concentration of cells is constant ($e_n + e_p + e_i = C_0$) we may drop one of e_n, e_p, and e_i equations. Here, we dropped the equation for e_i ($e_i = C_0 - e_n - e_p$). For initial conditions, $\begin{cases} e_n(0)=C_0 \\ e_p(0)=0 \\ e_i(0)=0 \end{cases}$. Additional details including a description of the model parameters (diffusion and production rates, diffusion length and abundance of paracrine factors), steady state analyses, and the numerical scheme are described in supplemental information. Quasi-steady state paracrine factor levels were solved using the finite element method using the MATLAB PDE (partial differential equation) toolbox (Mathworks, USA).

MATERIALS & METHODS

Immunofluoresence (for CD90 and phosphorylated-Smad2) and immunohistochemistry (for phosphorylated-Smad2) were performed on paraffin-embedded mouse or human prostate tissue sections as described (7, 19). A pathologist blindly evaluated immunohistochemical

staining. Primary stromal cells were isolated, cultured, and recombined with prostatic epithelial organoids as described (7, 19, 20). Tissue recombinations were performed as previously described (19, 21). For inhibition of DNA methylation, stromal fibroblasts were cultured for five days in the presence of 10 μM 5-aza-deoxycytidine (Sigma). $Tgfbr2^{fspKO}$ prostate stromal cells labeled with 2.0 μM CMFDA dye (Molecular Probes, Invitrogen) were co-cultured with Tgfbr2-flox stromal cells in 100 mm tissue culture dishes at 2×10^6 cells per dish for 20hrs. Cells were sorted on a BD FACS Aria II into cold RNA extraction buffer. DNase-I treated total RNA was isolated using the Qiagen RNeasy kit as instructed. Expression of SDF1, SFRP1, SFRP2, β-Actin, and GAPDH mRNA were evaluated by Quantitative Real-Time PCR (qRT-PCR). Amplification specificity was confirmed by melt-curve analysis and agarose gel visualization. Expression values were normalized for relative expression using the $\Delta\Delta C_T$ method. PCR primer sequences, numerical scheme, and steady state analysis methods are found in supplemental information. All procedures for human tissue acquisition and animal procedures were approved by the Vanderbilt University Institutional Review Board and Vanderbilt Institutional Animal Care and Use Committee, respectively.

RESULTS

Stromal heterogeneity: a two-step mechanism hypothesized for paracrine signaling-mediated tumor progression

To extend our study of stromal TGF-β signaling, phosphorylated-Smad2 expression was tested in a tissue microarray consisting of 80 human PCa samples. Independent of Gleason grade, phosphorylated-Smad2 was expressed homogenously throughout the epithelial compartment of all prostate samples examined. However, the stromal fibroblastic cells had heterogeneous phosphorylated-Smad2 staining in PCa tissues (Fig. 1A). Corresponding tissues of benign prostate hyperplasia (BPH) had a more homogeneous phosphorylated-Smad2 expression among stromal fibroblasts. Previous studies have suggested CD90 to be a marker heterogeneously expressed in PCa associated stromal cells (22). To further explore the role of stromal TGF-β signaling in PCa progression, we co-localized CD90 and phosphorylated-Smad2 expression by immunofluorescence in human PCa associated (N=10 patient samples, Gleason score range: 7–9) and non-cancer associated (N=6 patient samples) prostatic stromal fibroblastic cells. Interestingly, CD90 and phosphorylated-Smad2 expression was heterogeneous in the stromal cells of human PCa tissues (Fig. 1B). CD90 expression was generally limited to cancer associated stromal cells lacking phosphorylated-Smad2 expression. Stromal compartments associated with benign epithelia expressed both CD90 and phosphorylated-Smad2.

$Tgfbr2^{fspKO}$ mice were also found to have a heterogeneous loss of downstream Smad2 activation in stromal fibroblasts (Fig. 1C), partially attributable to the FSP1 promoter being active in only 40–60% of prostate fibroblasts. To determine the biological ramification of the observed stromal heterogeneity in TGF-β signaling, tissue recombination allografting experiments were conducted (N=6 grafts per group). Prostatic stromal cells from control $Tgfbr2^{floxE2/floxE2}$ mice (Tgfbr2-flox), and those from $Tgfbr2^{fspKO}$ (Tgfbr2-KO) were cultured. Although the loss of stromal heterogeneity is not observed *in vivo*, in the context of stromal-epithelial interactions, the culturing of prostatic stromal cells from $Tgfbr2^{fspKO}$ mice beyond six passages results in *Tgfbr2* knockout in 100% of the cells (19). The recombination of WT prostatic epithelial organoids with Tgfbr2-flox stroma under the renal capsule of syngeneic mice for 12 weeks yielded morphologically normal prostatic tissues (Fig. 2). In contrast, recombination of WT prostatic epithelial organoids with Tgfbr2-KO stromal cells resulted in PIN development in the same time period. The prostatic recombinants resulting from the equal mixture of Tgfbr2-flox and Tgfbr2-KO stromal cells with WT prostatic epithelia resulted in prostatic adenocarcinoma. The most immediate

interpretation of this striking observation is that the epithelia transform from normal to aggressive in two steps, where in the first step Tgfbr2-KO stromal cells contribute to initiating epithelial transformation and in the second step Tgfbr2-flox stromal cells contribute to the progression of initiated epithelia to an aggressive phenotype (invasion). Further, we believe it is likely that stromal-epithelial interactions are mediated by diffusive factors of some kind (23). Thus, we hypothesized a diffusive, two-step mechanism for epithelial transformation dependent upon stromal heterogeneity (TGF-β responsive and nonresponsive stromal cells). In step 1 of the hypothesized model, TGF-β non-responsive (Tgfbr2-KO) stromal cells produce a diffusive paracrine factor-1 (M_1), which cause epithelial cells to transform from normal to proliferative. In step 2, TGF-β responsive stromal cells (wild type and Tgfbr2-flox) produce a diffusive paracrine factor-2 (M_2), which supports the progression of proliferative epithelial cells to invade through the ductal basement membrane. For simplification, TGF-β responsive wild-type and Tgfbr2-flox stromal cells will be referred hence forward as WT.

A Computational Model Provides Proof-of-Concept for the Hypothesized Two-Step Mechanism of Tumorigenesis

A mathematical model describing epithelial and stromal fibroblastic cell signaling interactions was developed to test the viability of this proposed mechanism for epithelial transformation. Stromal and epithelial cell positions were modeled according to a histological section of mouse prostate (Fig. 3A) and simulations were used to investigate the predictions of a model for paracrine interaction. The model assumed epithelial cells transformed in response to threshold levels of stromal factors at steady-state concentrations (see the Quick Guide to Equations and Assumptions).

Implementation of the two-step mechanism in the computational model yielded results that qualitatively reproduced experimental observations over a wide range of simulation parameters. In simulations, the ratio of WT and Tgfbr2-KO stromal cells was varied from 0 to 1. The measured response variable for all simulations was the fraction of epithelial cells that transformed (Step 1, proliferative or Step 2, invasive). The fraction of transformed epithelial cells for a typical set of simulation parameters is shown in Fig. 3B. For 100% WT stromal cells (fraction altered stroma, FAS=0.00), there were no associated proliferative (Step 1) or invasive (Step 2) epithelial cells. For 100% Tgfbr2-KO stromal cells (FAS=1.00), there were only normal and proliferative epithelia. The computational model yielded invasion only at heterogeneous mixtures of stromal cells. Key model parameters (paracrine factor diffusion length $\boldsymbol{L}$, paracrine factor abundance $\boldsymbol{A}$, and paracrine factor threshold $\boldsymbol{T}$) could be varied to tune the fraction of epithelial cells that became proliferative or invasive; however, all parameters yielded results that were either identically zero or qualitatively similar to those shown in Fig. 3B, in which the fraction of proliferative epithelial cells increased monotonically from zero with the fraction of Tgfbr2-KO stroma (Step 1) and the fraction of invasive epithelia was non-zero only for intermediate fractions of Tgfbr2-KO stroma (Step 2). For example as a function of abundance of each paracrine factor (Fig. 3C), low abundance levels of M_1 (e.g., for $A_{M1} < 200$) resulted in no epithelial transformation and at higher abundance of M_1 the cells became proliferative. Finally, cells became invasive only if both M_1 and M_2 abundance levels were sufficiently high. In particular, the simulations demonstrated that wild-type stromal cells resulted in normal tissue, Tgfbr2-KO cells induced proliferative and hyperplasic epithelia, and only the heterogeneous mix of stromal cells induced invasive epithelia. This reproduction of the *qualitative* features of the experimental system provided a proof-of-concept for the hypothesized two-step mechanism of tumorigenesis.

Parameters for the computational model were chosen to match experimental results quantitatively, but parameters were not constrained uniquely. It was experimentally

observed that at a 1:1 WT : Tgfbr2-KO stromal fibroblastic cell ratio, the majority of epithelial cells became proliferative while a minority of epithelial cells became invasive. Model parameters could be tuned to match experimental epithelial transformation rates. Since increasing the diffusion length, increasing the abundance, and decreasing the threshold level all have the effect of increasing the fraction of cells that transform; this tuning was non-unique. In the Supplemental Information (SI), we describe how we tuned the parameters to find a non-unique set that generated and matched experimental results for the fraction of proliferative and invasive epithelial cells (SI Fig. 1, SI Fig. 2), and that the model predicted tissue morphology and stromal cell density influence upon epithelial progression toward cancer (SI Fig. 3).

Computational Model Predictions for the Relative Production of Stromal Factors

In our proof-of-principle consideration of the two-step model for tumorigenesis, we implemented the assumption that the paracrine factor produced by Tgfbr2-KO fibroblasts that supported proliferation (M_1) was not produced by WT fibroblasts at any level, and likewise that the paracrine factor produced by WT fibroblasts that supported invasion (M_2) was not produced by Tgfbr2-KO cells. However, candidate secreted factors dominantly expressed by fibroblastic cells that support proliferation and/or invasive cancer progression, include Wnt-3a and SDF-1, respectively (7, 19, 24) that are produced at non-negligible levels by both stromal cell types. Clearly, in the context of our two-step hypothesis for tumorigenesis, if Tgfbr2-KO fibroblasts were to support proliferation while WT fibroblasts did not, then a stromal factor supporting proliferation must be produced *dominantly* by the Tgfbr2-KO cells. Computational modeling could quantitatively determine how 'dominantly' M_1 must be expressed by the Tgfbr2-KO fibroblasts. Given relative production levels within these bounds, the model also made predictions regarding the diffusion range (measured as the characteristic diffusion length, the average distance traveled by a diffusing molecule during the average lifetime of a diffusing molecule) of the paracrine factors (M_1 and M_2).

Incorporation of experimental data (for the extent of epithelial transformation and the spatial scale of stromal-epithelial interaction) into the model established upper and lower boundaries for the threshold for epithelial transformation (see SI Fig. 4 and SI Table 1 for a more detailed explanation) and thereby the model was able to establish limits upon the relative n-fold increase in paracrine factor production and diffusion length required to obtain either no transformation (*Outcome A*) or epithelial transformation (*Outcome B*). Given a known fraction of epithelial transformation in *Outcome B*, the model predicted a lower bound for the fold difference in paracrine factor production between *Outcomes A* and *B*. If the fold difference in paracrine factor production was also known, the model made a more detailed prediction about the diffusion length of the invasive factor (M_2). Since the relative production of factors by each cell type may be measured experimentally, the permitted ranges predicted by the model may be used to evaluate whether putative factors for proliferation or invasion would be consistent with the diffusive two-step mechanism for tumorigenesis [as we describe below for Wnt-3a (M_1) and SDF-1 (M_2)]

Inconsistency of Wnt3a as a M_1 Paracrine Factor

Wnt-3a is a secreted factor dominantly expressed by stromal cells that is a candidate for supporting proliferation (7, 19, 24). Further, we identified that Tgfbr2-KO stromal cells up regulated Wnt signaling by the silencing of its antagonists, SFRP1 and SFRP2. Interestingly, the treatment of Tgfbr2-KO stromal cells with the DNA methylation inhibitor, 5-aza-deoxycytidine (5-aza-dC), restored SFRP1 and SFRP2 mRNA expression nearly to that observed for WT stromal cells (Fig. 4). Similarly, Tgfbr2-KO stromal cells epigenetically down-regulate SDF-1 expression, also restored by 5-aza-dC treatment. Thus, Tgfbr2-KO

stroma supported paracrine Wnt signaling, whereas, the WT stroma promoted SDF-1 expression.

In our tissue recombination allografting experiments, it appeared that more than 80±15% of epithelial cells transformed to become proliferative in the case of organoids with Tgfbr2-KO stromal cells. Our computational model thus predicted that the production of the factor in tissues supporting proliferation must be more than 12-fold that of tissues not supporting proliferation. However, we previously found that the production of Wnt-3a by WT stromal cells was 20% that of Tgfbr2-KO stromal cells (7) resulting in only a 3-fold difference in factor production in the tissues supporting and not supporting proliferation (Table 1). In other words, model parameters could not be found for M_1 (diffusion rate, decay rate, and thresholds for transformation) such that 80% of the epithelial cells would become proliferative at the 50/50 mixture of stromal cell types but 0% would become proliferative when the stromal cells are 100% normal. Indeed, we found that over a large parameter range (e.g., diffusion lengths ≤ 5000 μm), the model could not accommodate this level of M_1 production by Tgfbr2-KO stromal cells. This was demonstrated by the observation for any diffusion length $L \leq 800$ μm, a threshold cannot be found such that 80% of epithelial cells would become proliferative at the 100% Tgfbr2-KO mixture but 0% of epithelial cells would become proliferative at 100% WT stroma (Fig. 5A).

Consistency of SDF-1 as a M_2 paracrine factor

The chemokine, SDF-1/CXCL12 is implicated as a promoter of tumor epithelial progression to an invasive phenotype (25, 26). Expression of SDF-1 and its receptor (CXCR4) is positively regulated by TGF-β signaling (27, 28). Previously, we have performed microarray analysis of laser-capture microdissected (LCM) $Tgfbr2^{floxE2/floxE2}$ and $Tgfbr2^{fspKO}$ prostate stromal cells (data available in GEO database record GSE22130) isolated from mice (29). The data revealed the heterogeneity of gene expression of the stroma as well as a 77-fold increase in SDF-1 expression by $Tgfbr2^{fspKO}$ prostate stroma. This significant induction of SDF-1 mRNA expression in a heterogeneous stromal microenvironment is consistent with SDF-1 as a candidate paracrine factor in the promotion of PCa progression. Independently, SDF-1 mRNA levels in isolated cultures of WT and Tgfbr2-KO prostate stromal cells were quantified by real-time PCR. WT prostate stromal cells expressed 4-fold higher levels of SDF-1 mRNA than Tgfbr2-KO prostate stromal cells when grown alone in culture. The differential expression of SDF-1 here as compared to that measured by the microarray may be due to the presence of additional *in vivo* stromal cell types isolated by the LCM technique as compared to an isolated pure fibroblastic population grown in culture.

In our tissue recombination allografting experiments, it appeared that more than 20±5% of epithelial cells transformed to become invasive in the case of organoids with an equal mix of both stromal cells. Our computational model predicted that the production of the paracrine factor supporting invasion by the WT cells must be more than 2-fold that produced by the Tgfbr2-KO stroma. Thus, SDF-1 was consistent with M_2 in the two-step mechanism for tumorigenesis since the production of SDF-1 by Tgfbr2-KO cells is only 25% that of the WT cells. In other words, model parameters can be found for M_2 (diffusion rate, decay rate, and thresholds for transformation) such that 20% of the epithelial cells would become invasive at the 50/50 mixture of stromal cell types but 0% would become invasive when the stromal cells are 100% normal. For this production of SDF-1 by the Tgfbr2-KO cells, we found that the computational model predicts diffusion lengths greater than 24 μm (gray region, Fig. 5B). In this way, if a factor is consistent with being a factor in the two-step mechanism for tumorigenesis, the computational model predicts a range for the diffusion length.

Cooperativity of paracrine factor M_2

To quantify SDF-1 expression by the individual stromal fibroblastic cell, co-cultured mixtures of fibroblasts were separated by FACS sorting based on CMFDA (green) dye labeling of the Tgfbr2-KO cells, and SDF-1 mRNA quantified by qRT-PCR. The co-cultures were designed at the previously described ratios of Tgfbr2-KO and WT stromal cells (see Fig. 3B). FACS sorting of WT stromal cells grown in 75%:25% and 50%:50% co-culture with Tgfbr2-KO stromal cells revealed an approximately 5-fold and 8-fold increase in SDF-1 mRNA expression, respectively, compared to Tgfbr2-KO cells grown alone (Fig. 5C). Interestingly, SDF-1 mRNA levels of the Tgfbr2-KO stromal cells were elevated approximately 2-fold as a result of co-culture over Tgfbr2-KO cells grown alone. The results suggested that both WT and Tgfbr2-KO stromal cells may cooperatively induce production of one or more heterotypic stromal signaling factors resulting in increased SDF-1 mRNA expression. Inputting the experimentally measured relative production rates of SDF-1 for paracrine factor M_2 production levels in the computational model resulted in the experimentally observed rate of epithelial transformation (SI Fig. 5).

SDF-1 up-regulation by WT stroma in the case of a mixed stromal cell population compared with 100% WT stroma indicated that the presence of Tgfbr2-KO cells is communicated in some way to the WT cells, suggesting, for example, that there is an heterotypic stromal signaling factor (M_3) secreted by the Tgfbr2-KO cells that WT stromal cells respond to by up-regulating SDF-1 expression. Simulations tested the hypothesis that an M_3 factor could result in the cooperativity of SDF-1 expression (Fig. 5D). In these simulations, a geometry of cells were assumed in which stromal cells were confluent and arranged on a 2-D plate, as in the co-culture experiments. We modeled the production and diffusion of an M_3 expressed by Tgfbr2-KO cells that would cause the up-regulation of SDF-1 in WT cells at threshold levels. We identified rates of up-regulation and threshold levels that would result in experimentally measured production rates of SDF-1 for 0%, 25%, and 50% fraction of Tgfbr2-KO stroma. While we were able to find a fit within simulation error for the lowest fractions of Tgfbr2-KO stroma (light gray line, Fig. 5D), these model assumptions could not account for the decrease in SDF-1 production for higher levels of Tgfbr2-KO stroma. (While total production of SDF-1 by WT cells may be decreasing due to the decrease in their total number as the fraction of KO stroma increases, the production per wild type cell remains up-regulated.) In the same way that the increase in SDF-1 in the heterogeneous stromal mixtures logically argued for a threshold response to a factor produced by the Tgfbr2-KO stroma, the subsequent decreases in SDF-1 production for higher fraction of Tgfbr2-KO cells suggested a threshold response to a factor produced by the WT stromal cells. Assuming that SDF-1 was up-regulated in response to simultaneous threshold levels of an additional M_3 secreted by the Tgfbr2-KO stroma and an M_4 secreted by the WT stroma allowed finding a set of parameters that resulted in SDF-1 production levels that exactly matched experimentally measured levels within simulation error (dashed black line, Fig. 5D).

The potential for a Tgfbr2-KO-derived M_3 was tested in WT stromal cells. Microarray analysis of laser-capture microdissected prostate stroma from Tgfbr2-WT and Tgfbr2-KO mice revealed altered production of multiple secreted factors including the cytokines IL-1α (6-fold reduction), IL-β (4-fold reduction), and IL-6 (53-fold induction) by Tgfbr2-KO stroma in comparison to the Tgfbr2-WT stroma. Each of these factors have been implicated in the regulation of SDF-1 in the literature (30–32). Together these data imply that IL-1α, IL-1β, and Il-6 could be candidate heterotypicstromal signaling factors regulating SDF-1 expression. M_3 candidate factors that could up regulate SDF-1 (including IL-6, IL-1α and IL-1β) were tested on WT stroma. IL-1β increased SDF-1 expression over untreated WT cells by two-fold (Fig. 6A). Treatment of Tgfbr2-KO stromal cells with IL-1β increased SDF-1 mRNA levels nine-fold by qRT-PCR. Thus, IL-1β can be a candidate M_3 in the cooperativity mechanism between heterogeneous TGF-β responsive prostate stromal cells.

IL-1α and IL-6 had little effect on SDF-1 expression by either stromal cell type. Further, the biologic evidence for cooperative M_2 paracrine factor induction in a heterogeneous stromal microenvironment supports the computational model for a two-step paracrine-mediated tumor initiation and progression.

DISCUSSION

We describe a biological model for tumor initiation and progression based on heterogeneous stromal production of diffusive factors that mediate epithelial transformation. The aim was to account for a striking set of observations in which heterogeneity (but not homogeneity) of stromal fibroblastic cells was associated with tumorigenesis. Given obtained biological data for rates of epithelial transformation, the model predicted ranges for the relative fold production of factors. Given experimental measures of factor production, the model reported whether the factor was consistent with the biological model and predicted its diffusive range.

Given the ternary observations of the tissue recombination allografting experiments, it seemed unlikely that alternative hypotheses to the proposed mechanism (such as the epithelial progression does not occur in at least two steps or that these steps are not mediated by the stroma) would hold true. Certainly, the mechanism may be more complex, with added layers of interaction. Much literature supports that alterations in the stroma alone, independent of genetic events in the epithelium, can promote progression of neighboring epithelium to cancer (6, 21, 33–37). The step-wise nature of human carcinoma progression has been highlighted by the Knudson “Two Hit Hypothesis” (38). Paracrine-mediated cancer initiation and progression likely involves at least two distinct steps perpetuated by two or more factors produced by at least two independent cell types. Fibroblasts represent a heterogeneous cell population, some of which express FSP-1 and accordingly were knocked out for Tgfbr2 expression in the $Tgfbr2^{fspKO}$ mice. At least two fibroblastic cell sub-populations could be distinguished by CD90 expression (17) and we found CD90 expression coincided with heterogeneous Smad2 activity loss in human PCa associated fibroblasts. Similar fibroblastic heterogeneity in TGF-β responsiveness occurs in $Tgfbr2^{fspKO}$ mouse prostates and is likely functionally essential for the ensuing cancer progression.

The model is valid to the extent that stromal interactions were dominated by diffusive signaling. This biologically informed computational model was independent of specific paracrine factor production. M_1 or M_2 could represent individual or a combination of factors that result in epithelial proliferation and invasion, respectively. The computational model provided a quantitative measure of lower bounds for dominant factor production in terms of *n*-fold relative production. On the contrary, interactions are known to occur via extracellular matrix components and cell contacts. It is also possible that one step is dominantly mediated by a diffusive factor while the other is not. Observing an absence of epithelial transformation within the predicted diffusive range of the factor or the persistence of epithelial transformation after the introduction of barriers to diffusion could invalidate the model. An experiment to simultaneously test the candidacy of an M_1 or M_2 factor and the model would be to apply the factor exogenously with a steady concentration and measure the radius of epithelial transformation. The model is not explicitly time resolved as only cell response to steady state concentrations of signaling factors is considered, which was reasonable as steady state concentrations establish at fast time scales compared to cellular responses (17, 18). However, activities occurring at intermediate time scales, such as the gradual erosion of the basement membrane as a diffusion barrier in response to tumorigenic factors and epithelial effects on the stroma (for example, epithelial contribution to maintaining fibroblastic heterogeneity), could not be addressed by a steady-state model. Resolving the diffusion of paracrine factors over time to follow these intermediate activities,

including other mechanisms of cellular communication, and a 3-D representation of prostatic tissue are obvious extensions for a more detailed computational model of prostatic cancer progression.

With respect to details of factor production and number, the computational model is flexible and may be modified to accommodate any set of experimental observations regarding factor production for a report of the viability of the model with these factors. Here, the model was modified to accommodate non-linear, cooperative levels of M_2 production as observed in SDF-1 expression. Inputting the production levels phenomenologically, showed that SDF-1 was consistent with the model M_2. However, modeling the experimentally observed SDF-1 levels as a function of stromal heterogeneity supported heterotypic stromal communication, for example through additional signaling factors M_3 and M_4. However, it is particularly true for heterotypic stromal interactions that this communication need not be diffusive, such as through juxtacrine signaling.

The dichotomous view of TGF-β action as a tumor-suppressor in benign tissues and tumor-promoting in initiated cancer can involve the fibroblasts. TGF-β is tumor-suppressive in WT fibroblasts since it represses the secretion of Wnt-3a (and other Stat3 induced paracrine factors) (6, 7, 18, 32). TGF-β promotes SDF-1 production by fibroblasts and the expression of its receptor, CXCR4, in epithelial cells (33). The TGF-β non-responsive fibroblasts associated with cancerous epithelia express factors like IL-1β (M_3) to further SDF-1 production. Such TGF-β responsive heterotypic fibroblastic and stromal-epithelial signaling would support PCa onset and progression (Fig. 6B).

SUMMARY / CONCLUSION

Previous studies have emphasized the critical role of carcinoma-associated fibroblasts in cancer progression. The data suggest that the unaltered WT fibroblasts in the heterogeneous mixture of fibroblastic cells that make up the cancer stroma are not merely witnesses, but contribute to pro-carcinogenic cues that initiate epithelia, establishing a stromal field effect (39). Cooperativity of signaling within a heterogeneous stromal compartment would provide a mechanism whereby one could explain the multi-focal and polyclonal progression of PCa (39, 40). This can be envisioned where an initiating event in a particular duct confined prostatic epithelial cell causes a change in the neighboring stroma and in turn potentiates initiating change(s) in the adjacent epithelia at a somewhat distant ductal site(s).

Major Findings

A computational model was used to resolve a mechanism of prostate epithelial tumor initiation dictated by paracrine signaling. Model simulations and biological experiments supported fibroblast responsiveness to TGF-β as an initial tumor suppressor and subsequent mediator of tumor progression. TGF-β non-responsive stromal cells permitted the initial proliferative step. Cooperativity of both TGF-β non-responsive and responsive stromal cells was required for the secondary invasion step. Thus, stromal heterogeneity in TGF-β responsiveness enables a paracrine mediated tumorigenesis.

Supplementary Material

Refer to Web version on PubMed Central for supplementary material.

Acknowledgments

The authors wish to thank the members and advisors of the Vanderbilt University Tumor Microenvironment Network (VUTMEN) for helpful discussions throughout the course of this work. We thank Anne Kenworthy

(Vanderbilt University) for being supportive of Minchul Kang's assistance with this work. This work was supported by NIH/NCI RO1-CA108646 and U54-CA126505 (to N.A.B.) and a DOD-PRCP postdoctoral training grant W81XWH-08-1-0542 (to R.S.J.).

REFERENCES

1. Thesleff I, Vaahtokari A, Partanen AM. Regulation of organogenesis. Common molecular mechanisms regulating the development of teeth and other organs. Int J Dev Biol. 1995; 39:35–50. [PubMed: 7626420]
2. Bostwick DG, Pacelli A, Lopez-Beltran A. Molecular biology of prostatic intraepithelial neoplasia. Prostate. 1996; 29:117–134. [PubMed: 8700801]
3. Chung LW, Baseman A, Assikis V, Zhau HE. Molecular insights into prostate cancer progression: the missing link of tumor microenvironment. J Urol. 2005; 173:10–20. [PubMed: 15592017]
4. Alberti C. Genetic and microenvironmental implications in prostate cancer progression and metastasis. Eur Rev Med Pharmacol Sci. 2008; 12:167–175. [PubMed: 18700688]
5. Jackson RS 2nd, Franco OE, Bhowmick NA. Gene targeting to the stroma of the prostate and bone. Differentiation. 2008; 76:606–623. [PubMed: 18494814]
6. Bhowmick NA, Chytil A, Plieth D, Gorska AE, Dumont N, Shappell S, et al. TGF-beta signaling in fibroblasts modulates the oncogenic potential of adjacent epithelia. Science. 2004; 303:848–851. [PubMed: 14764882]
7. Li X, Placencio VR, Iturregui JM, Uwamariya C, Sharif-Afshar AR, Koyama T, et al. Prostate tumor progression is mediated by a paracrine TGF-β/Wnt3a signaling axis. Oncogene. 2008 In press.
8. Bacman D, Merkel S, Croner R, Papadopoulos T, Brueckl W, Dimmler A. TGF-beta receptor 2 downregulation in tumour-associated stroma worsens prognosis and high-grade tumours show more tumour-associated macrophages and lower TGF-beta1 expression in colon carcinoma: a retrospective study. BMC Cancer. 2007; 7:156. [PubMed: 17692120]
9. Anderson AR, Chaplain MA. Continuous and discrete mathematical models of tumor-induced angiogenesis. Bull Math Biol. 1998; 60:857–899. [PubMed: 9739618]
10. Alarcon T, Byrne HM, Maini PK. Towards whole-organ modelling of tumour growth. Prog Biophys Mol Biol. 2004; 85:451–472. [PubMed: 15142757]
11. Jiang Y, Pjesivac-Grbovic J, Cantrell C, Freyer JP. A multiscale model for avascular tumor growth. Biophys J. 2005; 89:3884–3894. [PubMed: 16199495]
12. Anderson, AC.; Mark; Rejniak; Katarzyna, A., editors. Single-Cell-Based Models in Biology and Medicine. Boston: Birkhause Verlag AG; 2007.
13. Alber MSK, MA.; Glazier, JA.; Jiang, Y. On cellular automation approaches to modeling biological cells. New York: Springer-Verlag; 2002.
14. Patel AA, Gawlinski ET, Lemieux SK, Gatenby RA. A cellular automaton model of early tumor growth and invasion. J Theor Biol. 2001; 213:315–331. [PubMed: 11735284]
15. Dormann S, Deutsch A. Modeling of self-organized avascular tumor growth with a hybrid cellular automaton. In Silico Biol. 2002; 2:393–406. [PubMed: 12542422]
16. Anderson AR. A hybrid mathematical model of solid tumour invasion: the importance of cell adhesion. Math Med Biol. 2005; 22:163–186. [PubMed: 15781426]
17. Basan M, Risler T, Joanny JF, Sastre-Garau X, Prost J. Homeostatic competition drives tumor growth and metastasis nucleation. HFSP J. 2009; 3:265–272. [PubMed: 20119483]
18. Goldman RDS, DL., editor. Live Cell Imaging: A laboratory manual. Cold Spring Harbor Laboratory Press; 2005.
19. Placencio VR, Sharif-Afshar AR, Li X, Huang H, Uwamariya C, Neilson EG, et al. Stromal transforming growth factor-beta signaling mediates prostatic response to androgen ablation by paracrine Wnt activity. Cancer Res. 2008; 68:4709–4718. [PubMed: 18559517]
20. Tuxhorn JA, Ayala GE, Smith MJ, Smith VC, Dang TD, Rowley DR. Reactive stroma in human prostate cancer: induction of myofibroblast phenotype and extracellular matrix remodeling. Clin Cancer Res. 2002; 8:2912–2923. [PubMed: 12231536]

21. Hayward SW, Wang Y, Cao M, Hom YK, Zhang B, Grossfeld GD, et al. Malignant transformation in a nontumorigenic human prostatic epithelial cell line. Cancer Res. 2001; 61:8135–8142. [PubMed: 11719442]
22. Zhao H, Peehl DM. Tumor-promoting phenotype of CD90hi prostate cancer-associated fibroblasts. Prostate. 2009; 69:991–1000. [PubMed: 19267366]
23. Cunha GR, Fujii H, Neubauer BL, Shannon JM, Sawyer L, Reese BA. Epithelialmesenchymal interactions in prostatic development. I. morphological observations of prostatic induction by urogenital sinus mesenchyme in epithelium of the adult rodent urinary bladder. J Cell Biol. 1983; 96:1662–1670. [PubMed: 6853597]
24. Klaus A, Birchmeier W. Wnt signalling and its impact on development and cancer. Nat Rev Cancer. 2008; 8:387–398. [PubMed: 18432252]
25. Cooper CR, Chay CH, Gendernalik JD, Lee HL, Bhatia J, Taichman RS, et al. Stromal factors involved in prostate carcinoma metastasis to bone. Cancer. 2003; 97:739–747. [PubMed: 12548571]
26. Waugh DJ, Wilson C, Seaton A, Maxwell PJ. Multi-faceted roles for CXC-chemokines in prostate cancer progression. Front Biosci. 2008; 13:4595–4604. [PubMed: 18508531]
27. Ao M, Franco OE, Park D, Raman D, Williams K, Hayward SW. Cross-talk between paracrine-acting cytokine and chemokine pathways promotes malignancy in benign human prostatic epithelium. Cancer Res. 2007; 67:4244–4253. [PubMed: 17483336]
28. Ao M, Williams K, Bhowmick NA, Hayward SW. Transforming Growth Factor-{beta} Promotes Invasion in Tumorigenic but not in Nontumorigenic Human Prostatic Epithelial Cells. Cancer Res. 2006; 66:8007–8016. [PubMed: 16912176]
29. Placencio VR, Li X, Sherrill TP, Fritz G, Bhowmick NA. Bone marrow derived mesenchymal stem cells incorporate into the prostate during regrowth. PLoS One. 2010; 5:e12920. [PubMed: 20886110]
30. Daly AJ, McIlreavey L, Irwin CR. Regulation of HGF and SDF-1 expression by oral fibroblasts--implications for invasion of oral cancer. Oral Oncol. 2008; 44:646–651. [PubMed: 17996483]
31. Garcia-Moruja C, Alonso-Lobo JM, Rueda P, Torres C, Gonzalez N, Bermejo M, et al. Functional characterization of SDF-1 proximal promoter. J Mol Biol. 2005; 348:43–62. [PubMed: 15808852]
32. McCandless EE, Budde M, Lees JR, Dorsey D, Lyng E, Klein RS. IL-1R signaling within the central nervous system regulates CXCL12 expression at the blood-brain barrier and disease severity during experimental autoimmune encephalomyelitis. J Immunol. 2009; 183:613–620. [PubMed: 19535637]
33. Barcellos-Hoff MH, Ravani SA. Irradiated mammary gland stroma promotes the expression of tumorigenic potential by unirradiated epithelial cells. Cancer Res. 2000; 60:1254–1260. [PubMed: 10728684]
34. Cheng N, Bhowmick NA, Chytil A, Gorksa AE, Brown KA, Muraoka R, et al. Loss of TGF-beta type II receptor in fibroblasts promotes mammary carcinoma growth and invasion through upregulation of TGF-alpha-, MSP- and HGF-mediated signaling networks. Oncogene. 2005; 24:5053–5068. [PubMed: 15856015]
35. Hill R, Song Y, Cardiff RD, Van Dyke T. Selective evolution of stromal mesenchyme with p53 loss in response to epithelial tumorigenesis. Cell. 2005; 123:1001–1011. [PubMed: 16360031]
36. Olumi AF, Grossfeld GD, Hayward SW, Carroll PR, Tlsty TD, Cunha GR. Carcinoma-associated fibroblasts direct tumor progression of initiated human prostatic epithelium. Cancer Res. 1999; 59:5002–5011. [PubMed: 10519415]
37. Phillips JL, Hayward SW, Wang Y, Vasselli J, Pavlovich C, Padilla-Nash H, et al. The consequences of chromosomal aneuploidy on gene expression profiles in a cell line model for prostate carcinogenesis. Cancer Res. 2001; 61:8143–8149. [PubMed: 11719443]
38. Knudson AG Jr. Mutation and cancer: statistical study of retinoblastoma. Proc Natl Acad Sci U S A. 1971; 68:820–823. [PubMed: 5279523]
39. Nonn L, Ananthanarayanan V, Gann PH. Evidence for field cancerization of the prostate. Prostate. 2009; 69:1470–1479. [PubMed: 19462462]

40. Mazzucchelli R, Scarpelli M, Cheng L, Lopez-Beltran A, Galosi AB, Kirkali Z, et al. Pathology of prostate cancer and focal therapy ('male lumpectomy'). Anticancer Res. 2009; 29:5155–5161. [PubMed: 20044631]

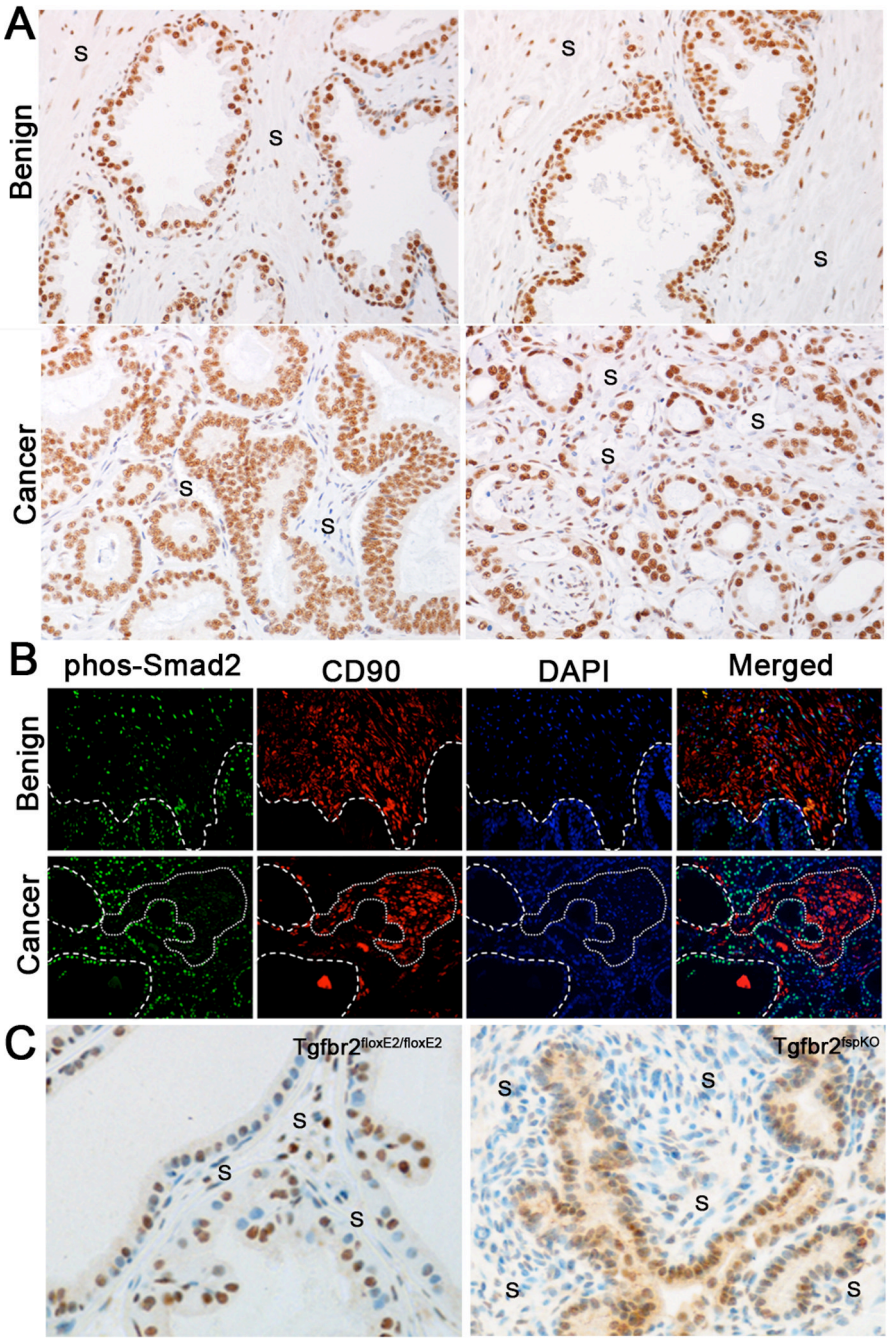

Figure 1. Stromal heterogeneity of human and mouse prostate tissues

A) Sample data of benign prostate hyperplasia (BPH) tissues suggest near homogeneous phosphorylated-Smad2 localization in the stroma (S). The lower and higher grade PCa tissues (left and right respectively) have similarly heterogeneous phosphorylated-Smad2 expression. B) Immunofluorescent staining demonstrating focal areas of increased stromal CD90 expression in human PCa (red, highlighted by dashed line) concurrent with loss of stromal phosphorylated-Smad2 expression (green). In comparison, there were greater uniformity in CD90 and phosphorylated-Smad2 in the BPH stromal tissue. C) There were heterogeneous phosphorylated-Smad2 localization in the prostate stroma of $Tgfbr2^{fspKO}$ compared to $Tgfbr2^{floxE2/floxE2}$ control mice.

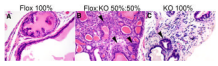

Figure 2. Percentage of WT and Tgfbr2-KO stroma in prostate tissue recombinant allografts promoted cancer progression

A) H&E of grafted WT prostatic epithelial organoids recombined with 100% Tgfbr2-flox prostate stromal cells had normal glandular architecture. B) There was observed progression to adenocarcinoma in grafts of WT prostatic epithelial organoids recombined with a 50/50 mixture of Tgfbr2-flox and Tgfbr2-KO prostate stromal cells. C) PIN lesions developed in grafts of WT prostatic epithelial organoids recombined with 100% Tgfbr2-KO prostate stromal cells. Arrowheads (B & C) indicate transformed epithelia.

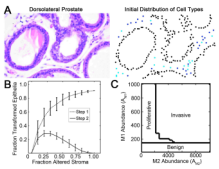

Figure 3. Establishment of a biologically informed computational model

A) H&E stained section of normal mouse prostate (left) was used to assign corresponding positions for simulated cells (right) assuming 50% Tgfbr2-KO stromal cells (black epithelia, blue WT stromal cells, and cyan Tgfbr2-KO stromal cells). B) Simulations indicated that stromal heterogeneity altered the proliferative and invasive potential of prostate epithelial cells, where greatest invasion occurred at heterogeneous mixtures of stromal cells and the extent of epithelial proliferation and invasion depended on the ratio of paracrine factor production and threshold response. The number of cells that became proliferative (Step 1, dashed line) and invasive (Step 2, solid line) was based on paracrine factor diffusion lengths ($\boldsymbol{L}_{M1}$=200 and $\boldsymbol{L}_{M2}$=300 μm), transformation response thresholds ($\boldsymbol{T}_{M1}$=0.0453 and $\boldsymbol{T}_{M2}$=0.3432 paracrine factor units), and fixed total paracrine factor abundance per cell source ($\boldsymbol{A}_{M1}$=$\boldsymbol{A}_{M2}$=10,000 paracrine factor units). Error bars indicate the standard error of 100 simulations. C) Phase diagram illustrating the final epithelial classifications as a function of Tgfbr2-KO cell M_1 abundance (y-axis) and WT cell M_2 abundance (x-axis) in a tissue at 50/50 mixture of WT and Tgfbr2-KO stromal cells. If the production rate of both paracrine factors was low relative to the transformation threshold, the cells remained normal. Paracrine factor diffusion lengths and thresholds for M_1 and M_2 were as in 3B.

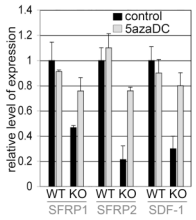

Figure 4. Epigenetic regulation of Wnt and SDF-1 signaling by TGF-β in prostate stromal cells

Quantitative RT-PCR revealed reversal of methylation induced silencing of SFRP1, SFRP2, and SDF-1 by 5-aza-dC treatment of Tgfbr2-KO stroma, comparable to WT stroma. Data are presented as mean ± S.D. and normalized to GAPDH.

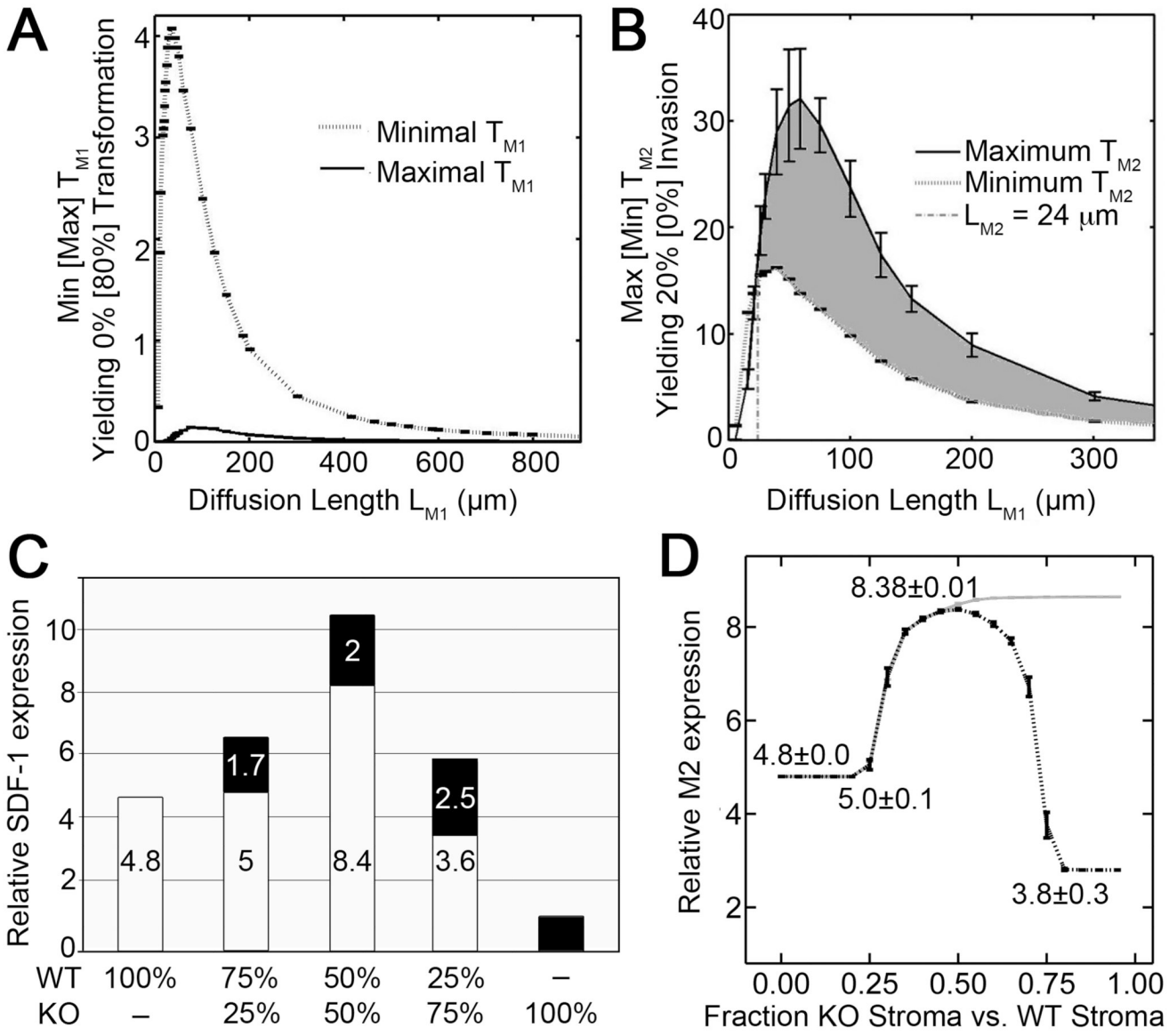

Figure 5. Computational modeling incorporating experimental data for putative paracrine factors predicted inter-stromal cell cooperativity for paracrine factor M_2 production

A) In simulations, WT stromal cells produced 20% of M_1 levels produced by Tgfbr2-KO stroma, modeling experimental data for Wnt-3a (M_1) production. The gap between the minimum (dotted line) and the maximum (solid line) thresholds illustrated that the model cannot yield experimental proliferation rates over this range of diffusion lengths. B) In simulations, Tgfbr2-KO stromal cells produced 25% of M_2 levels produced by WT stroma cells, modeling experimental data for SDF-1 (M_2) production. The area of overlap (shaded region) above the minimum (dotted line) and below the maximum (solid line) thresholds were consistent with experimental proliferation rates for diffusion lengths greater than L_{M2}=24 μm. Minima and maxima determination for A and B are described in supplemental information. C) SDF-1 (candidate M_2) expression by WT (white bar) and Tgfbr2-KO (KO, black bar) cell types was cooperatively elevated following co-culture as measured by qRT-PCR (normalized to β-actin, relative to KO expression). D) Simulation of M_2 production cooperativity assumed paracrine factors M_3 and M_4 expression by confluent WT and

Tgfbr2-KO stromal cells. Best-fit parameters were found to match data (in C) assuming first M_3 secretion by the Tgfbr2-KO stroma that resulted in SDF-1 induction by WT cells (gray line) and the added assumption of M_4 secretion by WT stroma augmented Tgfbr2-KO response to M_3 (dashed black line). Parameters for simulations are detailed in supplemental information.

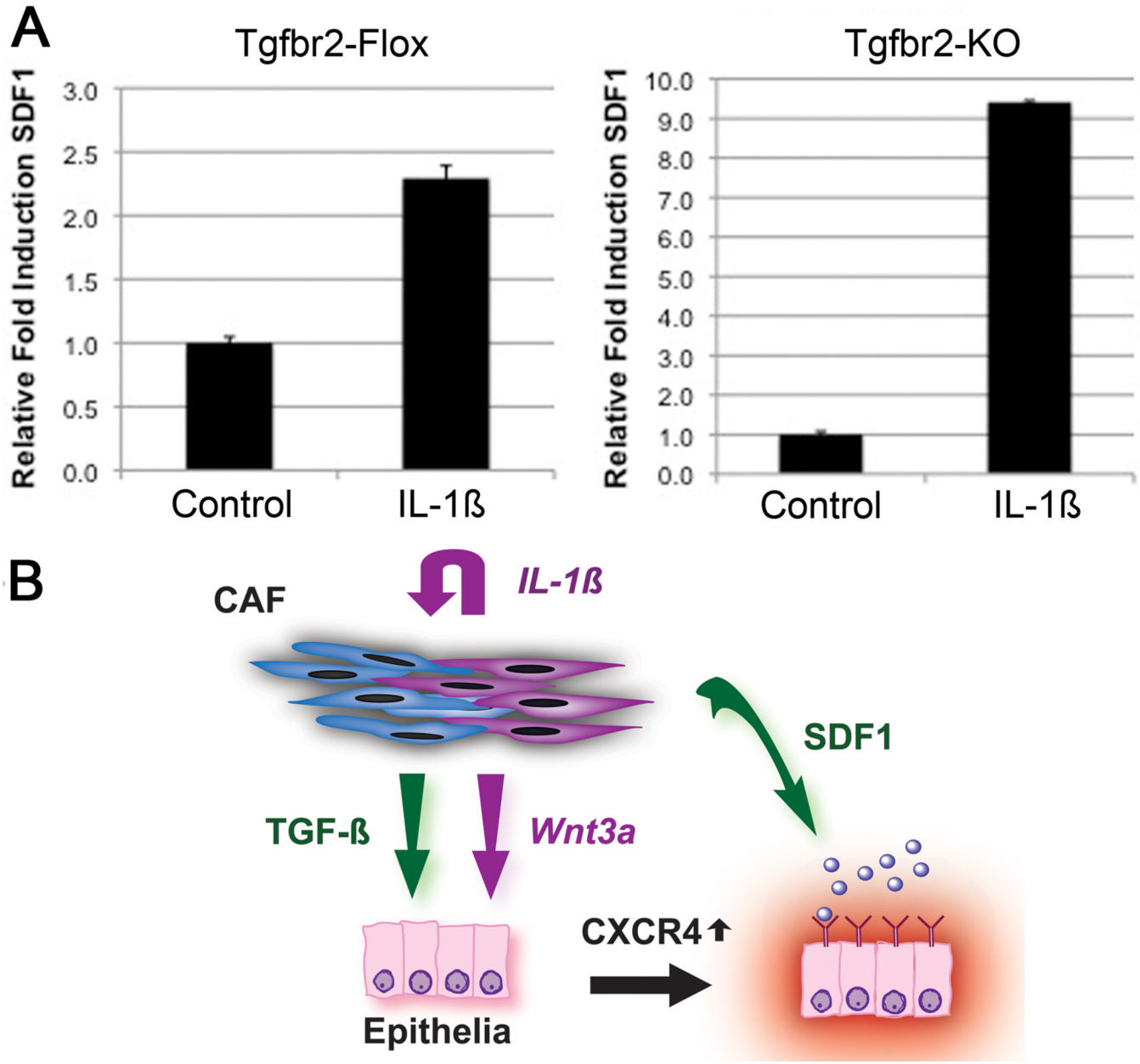

Figure 6. Paracrine signaling between stromal sub-types drives carcinogenesis

A) SDF-1 mRNA expression was measured in Tgfbr2-Flox and Tgfbr2-KO prostate stromal cells by qRT-PCR in response to treatment with the candidate M_3 heterotypic stromal signaling factor, IL-1β. B) A model of stromal TGF-β responsiveness driving prostate carcinogenesis.. Loss of stromal responsiveness to TGF-β, resulted in elevated production of TGF-β and Wnt-3a by the stroma. While increased Wnt paracrine signaling promoted epithelial proliferation, the increase in TGF-β in the microenvironment resulted in CXCR4 expression by the epithelium, subsequently increasing its sensitivity to SDF-1. WT and KO stroma cooperate to express elevated SDF-1, driving the progression of prostatic carcinogenesis.

TABLE 1
Morphogen M_1 Production by Stromal Cell Type

Number of stromal cells = N

Rate of M_1 Production by Altered Stromal Cells = k_1 (μm s^{-1})

Rate of M_1 Production by Normal Stromal Cells = 20% · k_1 (μm s^{-1})

	Fraction Altered Stroma	# of Normal Cells	# of Altered Cells	Average Cell Production of M_1 in Supportive or Non-Supportive Tissue
Experimental Outcome Type A: No Proliferation	0%	N	0	$=\frac{(20\%\cdot k_1)\times N+(k_1)\times 0}{N}$ $=20\%\cdot k_1$
Experimental Outcome Type B: 80% Proliferation	50%	$\frac{N}{2}$	$\frac{N}{2}$	$=\frac{(20\%\cdot k_1)\times \frac{N}{2}+(k_1)\times \frac{N}{2}}{N}$ $=60\%\cdot k_1$ $(=3\times(20\%\cdot k_1))$